Flash-Assisted Processing of Highly Conductive Zinc Oxide Electrodes from Water

Enrico Della Gaspera, Danielle F. Kennedy, Joel van Embden, Anthony S. R. Chesman, Thomas R. Gengenbach, Karl Weber, and Jacek J. Jasieniak**

Fabricating high-quality transparent conductors using inexpensive and industrially viable techniques is a major challenge toward developing low cost optoelectronic devices such as solar cells, light emitting diodes, and touch panel displays. In this work, highly transparent and conductive ZnO thin films are prepared from a low-temperature, aqueous deposition method through the careful control of the reaction chemistry. A robotic synthetic platform is used to explore the wide parameter space of a chemical bath system that uses only cheap and earth abundant chemicals for thin film deposition. As-deposited films are found to be highly resistive, however, through exposure to several millisecond pulses of high-intensity, broadband light, intrinsically doped ZnO films with sheet resistances as low as 40 $\Omega\ \square^{-1}$ can be readily prepared. Such values are comparable with state-of-the-art-doped transparent conducting oxides. The mild processing conditions (<150 °C) of the ZnO electrodes also enable their deposition on temperature sensitive substrates such as PET, paving the way for their use in various flexible optoelectronic devices. Proof-of-concept light emitting devices employing ZnO as a transparent electrode are presented.

1. Introduction

Solution processing is an accessible and versatile approach for depositing structurally and chemically controlled inorganic thin films.[1–6] For applications that require neat or composite nanostructured materials, e.g., battery electrodes, this processing method is employed almost ubiquitously.[7–9] However, for most thin-film-based optoelectronic applications, the material quality benchmarks are set by expensive, vacuum-deposited coatings. In comparison, solution processing is considered a "dirty" process because it involves precursors, stabilizers, and solvents, each of which can detrimentally impact the purity, surface chemistry, and microstructure of the deposited material. Arguably, the ability to control these factors through tailoring the reaction chemistry and processing conditions makes solution depositions more complex than vacuum-based ones, but also more powerful in view of the ultimate control that is offered.

Through careful optimization, coatings of a desired morphology, uniformity, structure, and functionality (optical, electrical, chemical, etc.) can be achieved. Consequently, solution-processed layers represent a viable industrial alternative to vacuum-based coatings in terms of capital investment, fabrication cost and quality of the prepared materials.[10–13] In spite of these clear advantages, the process of optimizing the chemistry involved in solution-based coatings requires the extensive screening and assessment of multiple parameters, which is extremely time- and labor-intensive. To this extent, advances in experimental automation may be used to overcome these challenges, by enabling for the rapid and continuous production of materials, as well as fast multiplexed screening of reaction parameters.[14–18] In this work, we focus on the chemical bath deposition (CBD) of transparent conductive ZnO thin films, showing how such a combinatorial approach can be used to optimize the deposition conditions of high grade functional thin film coatings (see **Figure 1**).

The CBD of ZnO films on seeded substrates from aqueous solutions is heavily influenced by the reaction temperature and pH, as well as the presence of ligands and/or dopants. Despite the large number of studies published on the controlled growth of ZnO from aqueous solutions, which led to the fabrication of various structures, such as dense films, nanowire arrays, rods, platelets, etc.,[19–25] the CBD of transparent and conductive (doped) ZnO has persisted as a major scientific challenge. With the rapidly increasing demand for low-cost flexible electronics, an area that is currently dominated by elementally scarce and expensive indium tin oxide (ITO), developing a facile, low-cost method for depositing a transparent conductive electrode (TCE) at low temperature is highly desirable and potentially lucrative.[26,27]

Recent reports on conductive ZnO thin films prepared via CBD have indicated progress toward achieving this goal.[28–31] In

Dr. E. Della Gaspera, Dr. D. F. Kennedy,
Dr. J. van Embden[+], Dr. A. S. R. Chesman,
Dr. T. R. Gengenbach, K. Weber, Prof. J. J. Jasieniak[++]
CSIRO Manufacturing Flagship
Bayview Ave
Clayton, Victoria 3168, Australia
E-mail: enrico.dellagaspera@csiro.au;
jacek.jasieniak@monash.edu
[+]Present address: School of Applied Science, RMIT University, Melbourne, Victoria 3000, Australia
[++]Present address: Department of Materials Science and Engineering, Monash University, Clayton, Victoria 3800, Australia

DOI: 10.1002/adfm.201503421

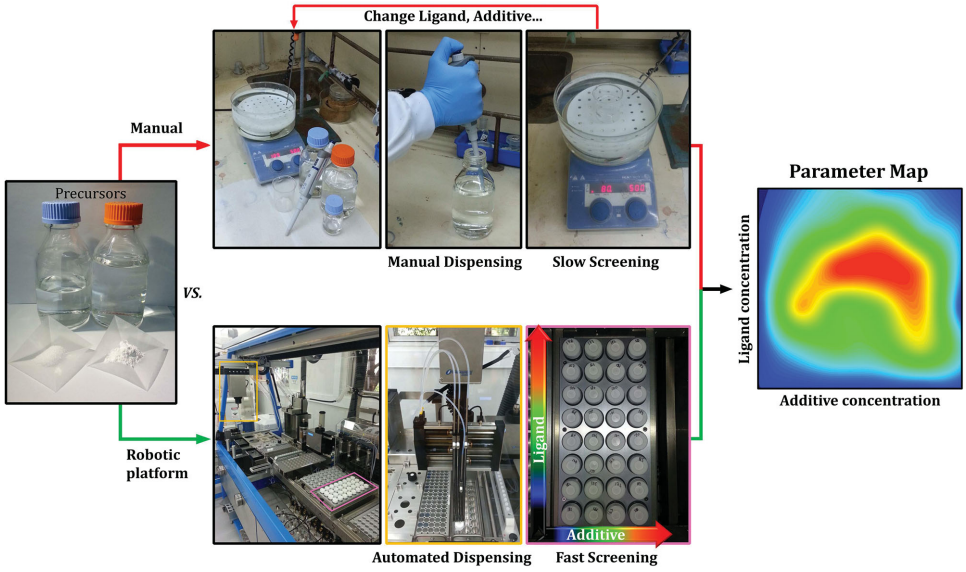

Figure 1. Manual versus automated deposition. Schematic flowchart of a traditional approach to the screening of reaction parameters in a chemical bath deposition (upper part) compared to the high-throughput, combinatorial approach adopted in this study (lower part).

those studies, however, the TCEs were prepared using aliovalent doping (Al or Ga) and often required a postdeposition annealing step at elevated temperatures. While enabling enhanced conductivity, this prevented such films from being deposited on temperature-sensitive substrates. Moreover, the presence of an extrinsic dopant during the CBD of ZnO is also known to heavily affect its growth characteristics.[24,32–34] To date, the most successful CBD process to deposit TCEs at low temperature has been for Al-doped ZnO (AZO):[35,36] Al ions were slowly and constantly supplied to the aqueous ZnO reaction bath in order to have a minimal effect on the growth of ZnO and obtain uniform, dense AZO films. The continual addition of Al ions during deposition caused an inherent vertical gradient to form within the resulting films. A more attractive synthetic method would utilize a simple one-step synthesis, wherein all the reagents are mixed together at the beginning of the reaction, thus avoiding the formation of any undesired gradients.

In this study we overcome the aforementioned issues by developing a low temperature, one-step CBD method to deposit transparent conductive ZnO films without the addition of extrinsic dopants. By introducing ammonium citrate as a ligand and an ammonium halide (in particular ammonium fluoride) as a buffering additive, we have achieved dense, highly transparent, and conductive ZnO films. Through this optimization, and with the assistance of an innovative high energy pulsed light exposure at room temperature, intrinsically doped ZnO films with transmittance above 90% in the visible range and sheet resistance of 40 $\Omega\,\square^{-1}$ are demonstrated. To validate their use as transparent electrodes, these ZnO films are employed within solution-processed, ITO-free optoelectronic devices.

2. Results and Discussion

To investigate the parameter space of the CBD protocol for the synthesis of ZnO thin films, we used the Chemspeed SWINGXL automated synthesis platform. Details are presented in Figure S1 and Table S1 (Supporting Information). For the aqueous bath, we used zinc nitrate as the zinc source, ammonium citrate as the ligand and ammonium fluoride as the additive. Each chemical was dissolved in water at an appropriate concentration (see the Experimental Section for details) to give the stock solutions. We analyzed the effect of i) the molar ratio between ammonium citrate and zinc nitrate, defined as r_C; ii) the molar ratio between ammonium fluoride and zinc nitrate, defined as r_F; iii) the bath temperature; iv) the reaction time; and v) the zinc concentration. A summary of the parameters investigated with their respective ranges is reported in Table S2 (Supporting Information).

2.1. Thickness, Structure, and Morphology

At the start of our investigation into the reaction parameters, we focused on the thickness and the morphology of the deposited ZnO. **Figure 2**a shows the thickness of the ZnO films deposited at 80 °C as a function of r_C and r_F. When the citrate amount is high (r_C = 0.5), no deposition of ZnO is observed, regardless of the r_F value. This is due to the high binding affinity of citrate anions to zinc cations, which prevents their subsequent reaction to form ZnO. At lower citrate levels (i.e., $r_C \leq 0.2$), the thickness of the films becomes dependent on the values of both r_C and r_F. As a general trend, in this regime an increased film thickness is achieved at lower r_C and higher r_F values. The presence of citrate and fluoride in the bath also affects the morphology of the growing films (Figure 2b,c). All samples are strongly textured, showing elongated, wire-like grains that are aligned in a direction orthogonal to the substrate due to preferential growth along the *c*-axis of the ZnO hexagonal wurtzite cell. The high surface energy of the Zn-terminated (0001) and O-terminated $(000\bar{1})$ surfaces causes the formation of long ZnO grains having such surfaces as basal planes.[22,37] This texturing

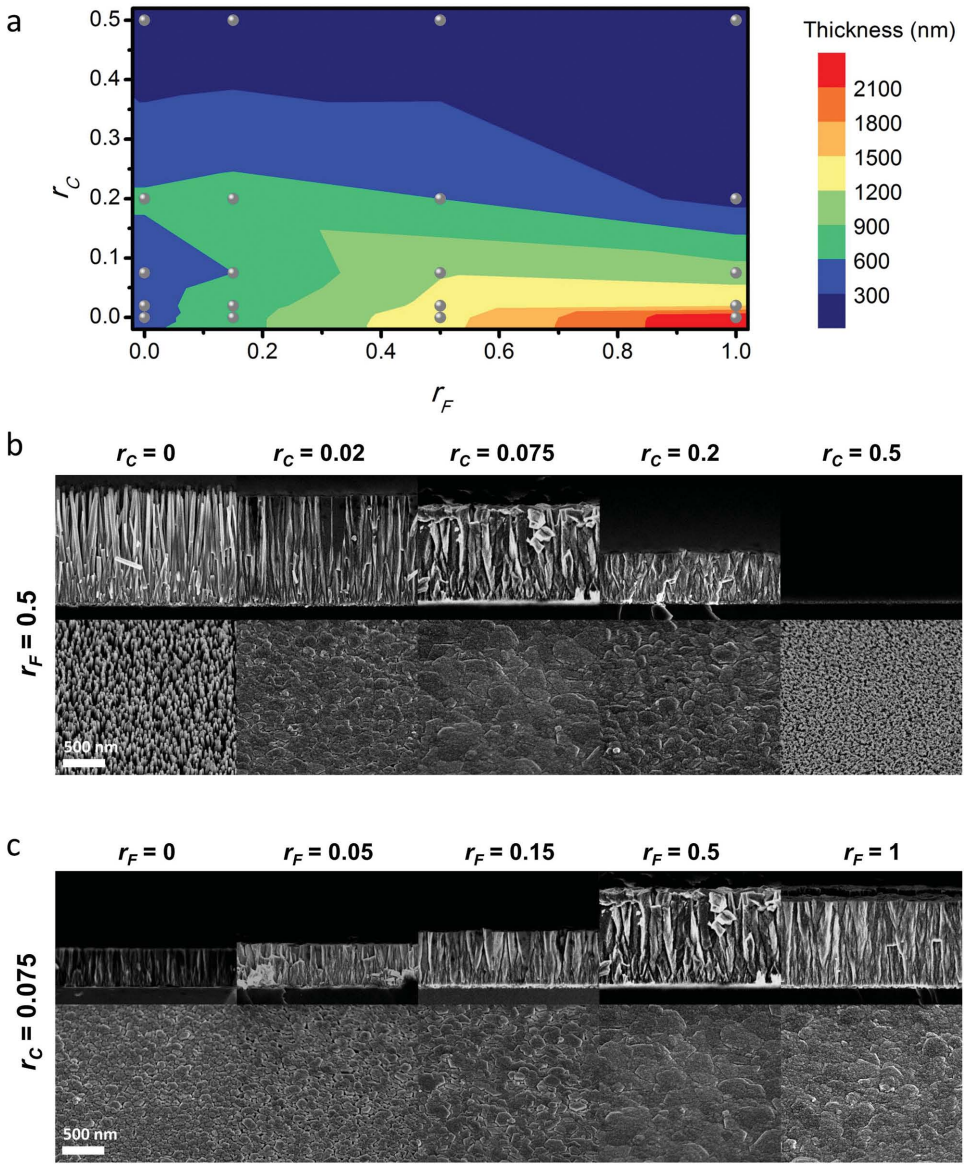

Figure 2. Effect of the amount of ammonium citrate and ammonium fluoride. a) Contour plot of ZnO thickness as a function of r_C and r_F. The gray circles identify the experimental points. The individual plots of thickness versus r_C and r_F are presented in Figure S3 (Supporting Information). b) SEM images in cross section (upper images) and top view (lower images) of ZnO films prepared with $r_F = 0.5$ as a function of r_C. The sample synthesized with $r_F = 0.5$ and $r_C = 0.5$ shows only the presence of the ZnO seed layer. c) SEM images in cross section (upper images) and top view (lower images) of ZnO films prepared with $r_C = 0.075$ as a function of r_F. All depositions were carried out at 80 °C for 1 h.

is responsible for the dominant (002) diffraction peak being observed in the X-ray diffraction (XRD) patterns (Figure S2, Supporting Information).

The citrate ligand plays a pivotal role in controlling i) the reactivity of the zinc cations in solution and ii) the lateral growth rate of the forming ZnO thin film. Evidence for the latter stems from chemical bath depositions performed without ammonium citrate, for which it is known that ZnO grows as an array of long, separated, and vertically aligned nanowires. This arises because citrate anions have a strong affinity for the polar (0001) and $(000\bar{1})$ surfaces of ZnO, which kinetically restricts growth along these planes, while enhancing the relative growth along the ⟨002⟩ direction.[20] These functional roles of citrate enable the formation of dense ZnO thin films at intermediate r_C values and ultimately explain the decrease in ZnO thicknesses for high r_C values (see Figure 2b). Notably, unlike the citrate ligand, ammonium fluoride does not have a strong influence on the morphology of the growing films (Figure 2c).

Similar trends to those described above are also observed for samples prepared at 70 and 90 °C, with those samples synthesized at higher temperature being thicker and rougher on average (Figures S4 and S5, Supporting Information). At the lowest temperature investigated in this study (60 °C), high values of r_F also caused a decrease in thickness, and the r_C value at which deposition is suppressed was lowered from 0.5 to 0.2. This validates the claim that ammonium citrate directs

ZnO growth and that this process is kinetically controlled. In this case, the initial growth rate can be readily modified without changing the final microstructure (dictated largely through r_C) by changing the Zn concentration (Figure S6, Supporting Information). The final thickness obviously depends on the duration of the CBD, with the thickness increasing with reaction time (Figure S7, Supporting Information). As a result, through a suitable choice of deposition time, reaction temperature and zinc precursor concentration, the thickness of the ZnO coatings can be precisely adjusted (Figure S7, Supporting Information).

2.2. Optical and Electrical Properties

The typical transmittance spectrum of one of our ZnO coatings (r_C = 0.075, r_F = 1, T_{growth} = 80 °C) is presented in **Figure 3**a. Conducive to its use as a transparent electrode, it exhibits a transmittance of over 90% across the visible and near infrared (NIR) regions. The observed interference fringes overlaying the profile are directly related to the smooth nature of the ZnO and the accompanying multiple light reflections occurring at the air/ZnO/glass interfaces. Across all of the samples investigated, exceptions to such high transmittance cases are typically restricted to samples prepared without ammonium citrate (Figure S8, Supporting Information) and/or those synthesized at 90 °C (Figure S9, Supporting Information), both of which exhibit scattering contributions across the visible spectrum due to their structural length scales being comparable to the wavelength of light. Importantly, regardless of their optical characteristics, none of the as-prepared ZnO samples exhibited appreciable electrical conductivity, with the most conductive samples showing sheet resistance values on the order of ≈1 MΩ $\square^{-1}$.

It is well known that ZnO can be photodoped upon exposure to UV light. Current evidence suggests that this process relies on the UV-induced photooxidation of oxygen, water, and organic molecules adsorbed on the ZnO surface. In this process, photogenerated holes are transferred to these adsorbates, which create an excess of electrons in the conduction band and, thus, increase the conductivity of n-type ZnO.[38,39] Here we show that exposure to UV light has a dramatic impact on the properties of our CBD-grown ZnO films. Considering the example shown in Figure 3, after exposure to UV light, a strong IR absorption appears in the transmission spectrum. This feature is related to the increased number of free carriers in the photo-doped ZnO. Concurrent with this effect, a blueshift of the optical band gap from ≈3.4 to ≈3.6 eV is also seen, consistent with the Burstein–Moss effect. Such phenomena have been observed previously in extrinsically doped ZnO colloidal nanocrystals and thin films, and ascribed to dopant-induced generation of free carriers.[40–42] Notably, the films remain highly transparent across the visible spectral region. This makes them attractive for application as transparent conductors and NIR reflective coatings (heat mirrors).

Accompanying the observed changes in the optical features of our ZnO films is a variation of their electrical properties. We measured the sheet resistances of all the prepared samples before and after UV exposure, and compared them to their average transmittance in the 400–800 nm range (Figure 3b). In this plot, the area of desired performance for a transparent conductor is the top left corner, corresponding to high transparency and low sheet resistance. The figure shows a clear drop in resistance of ≈2–3 orders of magnitude for many of the prepared ZnO films after UV exposure, thus validating the origin of the IR plasmonic features in the optical absorption spectra.

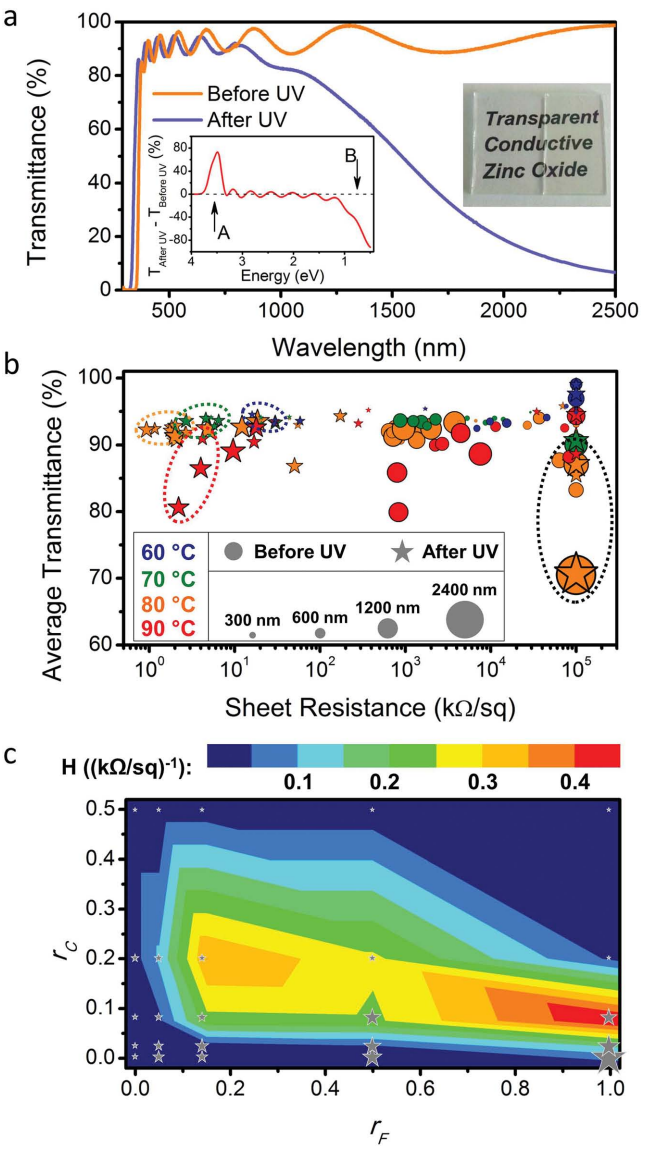

Figure 3. Optical and electrical characterization of ZnO films. a) Transmittance spectra of a ZnO film prepared from a bath with r_C = 0.075 and r_F = 1 at 80 °C before (orange line) and after (purple line) exposure to UV light. The left inset shows the UV-induced variation in transmittance on an energy scale, highlighting A) the blueshift of the optical band gap and B) the IR absorption, with minimal effect on the visible transmission. The right inset shows a digital picture of a glass slide (left) and a ZnO sample on glass (right). b) Plot of average visible transmittance versus sheet resistance for the samples prepared in this study, where the circles correspond to the as-prepared films and the stars are the values after UV exposure. The bath temperatures are color coded, and the size of the symbols represents the samples thickness. c) Contour plot of the Haacke value (in (kΩ $\square^{-1}$)$^{-1}$)) as a function of r_C and r_F after UV exposure for the samples synthesized at 80 °C. The individual plots of the Haacke value versus r_C and r_F are presented in Figure S10 (Supporting Information).

Of all the samples, CBD performed at 80 °C provides the best combination of transparency and conductivity. Samples deposited at lower temperatures suffer from poor conductivity, while samples prepared at 90 °C suffer from a reduced transparency. It is worth noting that the samples synthesized at 70 and 80 °C that show poor transmittance (samples encompassed by the black dotted circle), are composed of isolated nanowires that partially scatter light in the visible range (Figure S8, Supporting Information). Notably, some of the highly resistive samples did not show an increase in conductivity following the UV exposure, which stems from the fact that these samples were at the detection limit of our measurement system (100 MΩ $\square^{-1}$).

To present the data in a more universal manner, which naturally accounts for both electrical and optical properties, we used the Haacke value, H, as a figure of merit.[43] Widely adopted for evaluating transparent conductors, it is defined as

$$H = \frac{T^{10}}{R_s} \quad (1)$$

where T is the optical transmittance (usually measured at 550 nm, though in this case we adopted the average across the 400–800 nm range) and R_s is the sheet resistance. The higher the Haacke value, the better the combination of transparency and conductivity. Despite their high transparency, samples synthesized at 60 °C have a very low H due to their high electrical resistivity. At 90 °C, even though the samples are conductive, the reduced transparency results in low Haacke values (Figure S10, Supporting Information). The highest Haacke value of ≈0.46 (kΩ $\square^{-1}$)$^{-1}$ is obtained for samples deposited at 80 °C (Figure S11, Supporting Information), which supports the results presented in Figure 3b.

The plots presented in Figure 3b and (Figure S10–S11 (Supporting Information) highlight the best deposition temperature to achieve high-performance transparent conductors. However, there is a large variation in performance across the different samples that is related to the specific deposition conditions, namely through variations of ligand and additive concentrations. Focusing on the samples deposited at 80 °C, we present in Figure 3c the effect of r_C and r_F on the Haacke figure of merit after UV exposure. Samples prepared with the highest amount of ammonium citrate (r_C = 0.5) and without ammonium citrate (r_C = 0) have the lowest Haacke value, on the order of 10^{-8} (Ω $\square^{-1}$)$^{-1}$ or less. In the former case, the high citrate concentration suppresses the deposition of ZnO, and therefore the high resistance of the very thin (<50 nm) sol–gel seed layer is responsible for the observed results. In the latter case, in the absence of ammonium citrate the samples are arrays of aligned nanowires rather than dense films. Consequently, even given reasonable electrical conduction along the axis of the nanowires, there is no lateral conduction, which results in high sheet resistance values and low H values. Such samples also have a lower visible transmittance, which contributes to a further reduction in this figure of merit. At intermediate r_C values, a band emerges in which H tends to increase with the amount of ammonium fluoride present in the chemical bath (see Figure 3c and Figure S10, Supporting Information).

While the effect of ammonium citrate is readily linked to the growth of ZnO and its morphology, the role of ammonium fluoride is less clear. To elucidate this, we used X-ray photoelectron spectroscopy (XPS) to probe the surface chemical composition, as well as oxidation states and chemical bonding for samples prepared under the same reaction conditions, but with different r_F values (**Figure 4** and Table S3, Supporting Information). The

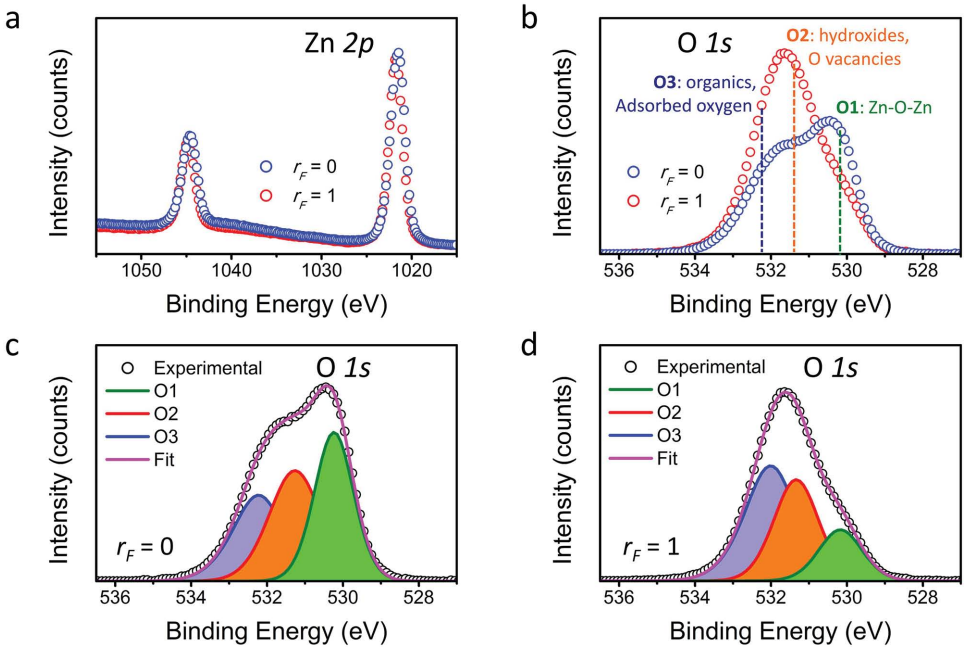

Figure 4. XPS characterization of ZnO films. X-ray photoelectron spectra of a) Zn 2p region and b) O 1s region for two ZnO films prepared with r_C = 0.075 and r_F = 0 (blue dots) and r_F = 1 (red dots). The expected peak position for the O1, O2, and O3 components of the O1s peak are also reported. c,d) The fitting of the three components of the O1s peak for the samples prepared with r_F = 0 and r_F = 1 are reported, respectively.

O 1s peak was used for comparison as it is highly susceptible to subtle chemical changes in metal oxides.[44] The results indicate that the O 1s signal is composed of a series of contributions, which can be assigned to O^{2-} ions within the ZnO lattice (O1 component), hydroxides or oxygen atoms residing in oxygen-deficient environments (O2 component), and to adsorbed oxygen or organic contaminants (O3 component).[44] Based on this analysis it is apparent that samples prepared using ammonium fluoride possess a more oxygen-deficient ZnO structure. This nonstoichiometric composition is responsible for the improved electrical properties compared to samples prepared without NH_4F. Notably, samples prepared without this additive also remain slightly oxygen deficient, as evident from an O/Zn ratio <1 (Table S3, Supporting Information), which differs from our previously reported CBD process of *i*-ZnO using different chemistry, where the O/Zn ≈ 1.[25] This highlights that the CBD used here (basic pH, presence of ammonium citrate) is not suitable to prepare resistive, *i*-ZnO films, but rather is tailored toward nonstoichiometric films.

Similar results in terms of optical/electrical properties and increased oxygen vacancies were also obtained when using ammonium chloride instead of ammonium fluoride as an additive. It is worth noting that no evidence of halogen incorporation within the ZnO films has been detected with either XPS, X-ray fluorescence, or energy-dispersive X-ray spectroscopy, suggesting that the role of the ammonium halide is not to generate additional charge carriers by displacing O^{2-} with halide ions, as occurs in commonly used transparent conducting oxides, such as fluorine doped tin oxide and F^- or Cl^- doped ZnO.[45–47]

Having explored a large parameter space (see Table S4, Supporting Information, for a summary of selected reactions), we have chosen the best conditions to grow highly transparent and conductive ZnO films. The transmittance and sheet resistance values of our champion films as a function of light exposure are presented in **Figure 5**. Examination of Figure 5a reveals that UV treatment causes an increase in the plasmonic absorption, even after very short exposure times, and a progressive blueshift of the optical band gap of ZnO (Figure S12, Supporting Information). Concomitantly, the sheet resistance decreases and the Haacke value increases (Figure 5c). UV exposure is most effective at the beginning of the treatment (1–2 min), with its effect progressively reduced with further exposure. After prolonged UV exposure (20 min) we achieved a minimum sheet resistance of ≈800 Ω $\square^{-1}$, with the sample remaining highly transparent in the visible range. A Haacke value of 6.5×10^{-4} $(\Omega\ \square^{-1})^{-1}$ was calculated, which is remarkably low for a low temperature, solution processed, intrinsically doped ZnO thin film. However, such a value is still at least an order of magnitude lower than the current state-of-the-art transparent conducting oxides. Moreover, several minutes of UV exposure are required to achieve this level of conductivity.

To address these issues, we replaced the UV treatment with flash illumination using a high-intensity xenon lamp with millisecond light pulses. With only five flashes (2 ms each, total exposure time of 10 ms) we could match the performances obtained

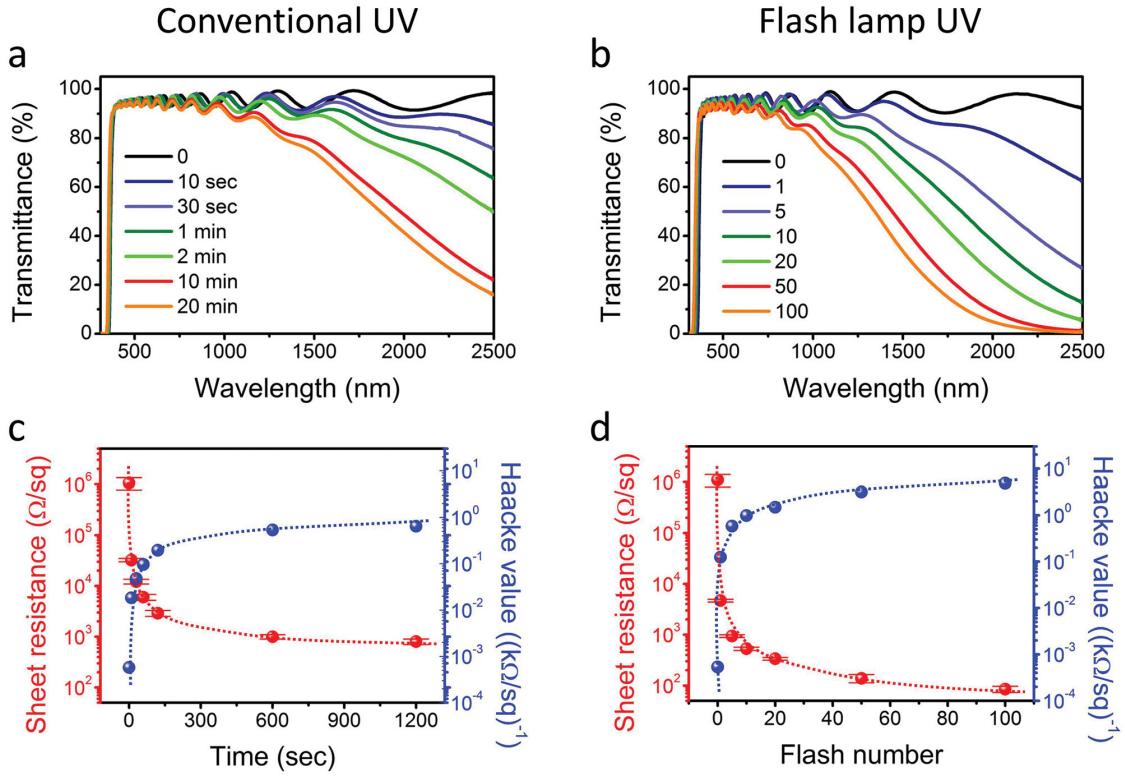

Figure 5. Comparison between conventional and flash lamp UV exposure. a,b)Transmittance spectra and c,d) sheet resistance and Haacke value for ZnO samples prepared with $r_C = 0.075$ and $r_F = 1$ according to a,c) conventional UV exposure time and b,d) number of flash lamp pulses. The error bars represent one standard deviation. Note that panels (c) and (d) have the same vertical scales. The dotted lines in (c,d) are included as a guide for the eye.

after 20 min of conventional UV exposure. By increasing the number of flashes we achieved a much lower sheet resistance (85 Ω $\square^{-1}$), wider optical band gap (Figure S12, Supporting Information), and very strong IR absorption, while still maintaining high transparency in the visible range (Figure 5b,d). The Haacke value associated with this sample is 4.9×10^{-3} $(\Omega \square^{-1})^{-1}$, which meets the requirements for a transparent electrode in conventional optoelectronic devices such as touch panel displays and LEDs.[48,49] In addition, utilizing thicker ZnO films by simply increasing the deposition time to 3 h (final thickness of ≈2.6 µm) we achieved a sheet resistance of 40 Ω $\square^{-1}$, with an associated Haacke value of 7×10^{-3} $(\Omega \square^{-1})^{-1}$ after 50 flash lamp pulses (100 ms of total UV exposure), as shown in Figure S13 (Supporting Information). To the best of our knowledge, this figure of merit is the best reported for a solution-processed, intrinsically doped ZnO film, and places our ZnO alongside the best performing transparent conducting oxides. Consistent with this photodoping mechanism, the effect induced by the UV exposure is found to be only retained while the sample is kept under an inert (e.g., nitrogen, argon) atmosphere, with a gradual increase in resistivity being observed after prolonged exposure to air due to the readsorption of oxygen and water molecules on the ZnO surface (Figure S14, Supporting Information).[39] Notably, this is not a major issue considering that many optoelectronic devices require encapsulation to ensure long-term stability of the active layers for operation in ambient conditions.

The versatility of the low-temperature process outlined here is further demonstrated by the deposition of ZnO coatings onto plastic substrates, as for example poly(ethylene terephthalate) (PET). In this case, lower annealing temperatures were used for the seed deposition (100–140 °C, compatible with the thermal stability of PET), while the CBD was carried out using our optimized experimental method. Using this procedure, highly transparent ZnO films were successfully deposited on PET. Likewise, upon UV exposure they exhibit characteristics similar to those observed for films deposited on rigid glass substrates (Figure S15, Supporting Information).

2.3. Device Fabrication

To demonstrate the quality and efficacy of our low-temperature, solution-processed transparent conducting ZnO films, we prepared organic light emitting devices (OLEDs) using these ZnO films as transparent electrodes and a yellow light emitting polymer (Super Yellow PDY-132, see the Experimental Section) as the emissive layer. All the layers, excluding the Ca/Al metal cathode, were solution processed. As can be seen from **Figure 6**, functional devices with high luminance, bright yellow color and uniform emission across the pixels were fabricated. In comparison to standard ITO/glass-based devices, these did possess higher turn-on voltages due to the larger energy offset between poly(3,4-ethylenedioxythiophene):poly(styrene sulfonate) (PEDOT:PSS) and ZnO compared to ITO (see Figure S16 in the Supporting Information); however, their operation validates the use of our ZnO as a suitable transparent electrode for optoelectronic devices.

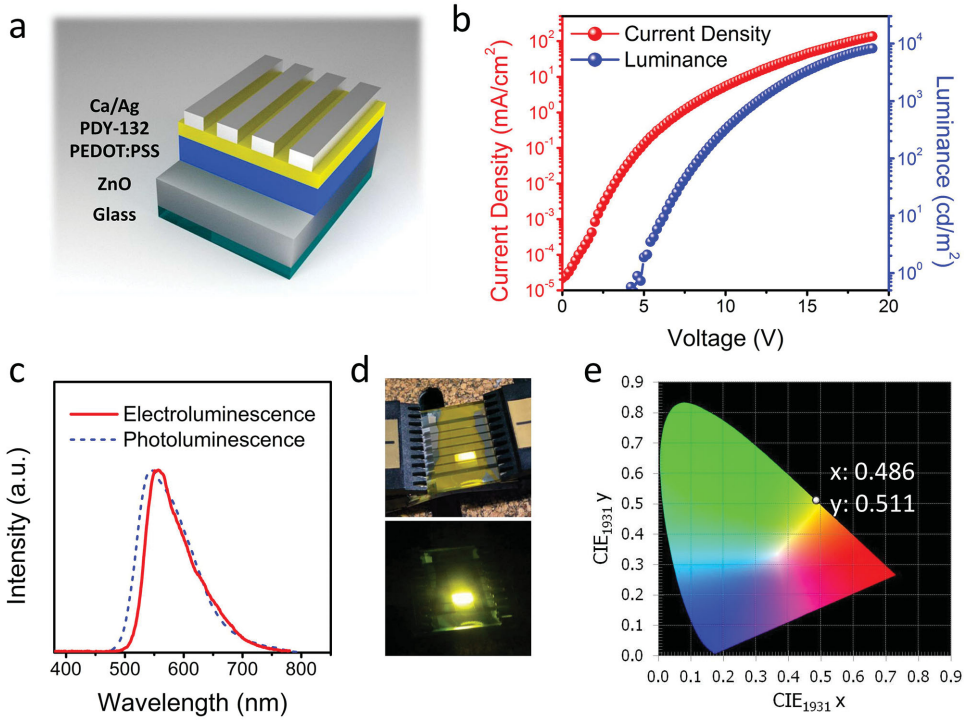

Figure 6. Characterization of yellow OLEDs prepared using ZnO as a transparent electrode. a) Structural schematic; b) current density and luminance plots versus voltage; c) electroluminescence emission spectrum and comparison with the photoluminescence emission spectrum of a PDY-132 film; d) digital photographs of the working device under ambient light (top) and in the dark (bottom); and e) CIE 1931 chromaticity diagram highlighting the coordinates for the prepared yellow OLEDs.

3. Conclusion

In conclusion, we have developed highly conductive and transparent ZnO films using a simple one-step aqueous bath deposition method without the need for extrinsic doping. We extensively screened the parameter space of the chemical bath system using an automated synthetic platform. Utilizing this platform we were able to rapidly evaluate the effect of key variables such as temperature, deposition time, ligand concentration (ammonium citrate), and additive concentration (ammonium fluoride) on the optical, electrical, and structural properties of the as-deposited thin films in order to arrive at an optimized protocol. These optimal reaction conditions were used to deposit highly transparent and conductive ZnO films. Exposure to millisecond pulses of UV light was used to greatly enhance the electrical conductivity of our ZnO films, with a champion Haake value of 7×10^{-3} $(\Omega\ u^{-1})^{-1}$, being comparable to state-of-the-art transparent conductive oxides. Notably, such films were obtained using a scalable CBD technique without the use of any high temperature processing steps. The films fabricated here represent the foundation for using simple binary metal oxides as transparent conductive electrodes. Their ability to be deposited on plastic enhanced their versatility and poises them for commercial translation into a variety of flexible electronic devices. Proof-of-concept depositions on plastic substrates and fabrication of ITO-free organic light emitting devices confirm the quality and adaptability of our process, which constitutes a great advance toward the fabrication of reliable, cost-effective, and high-performance flexible electronics and optoelectronic devices in general.

4. Experimental Section

Chemicals: All chemicals were reagent grade and were used without further purification. Zinc nitrate hexahydrate (98%), ammonium citrate (98%), and ethanolamine (99%) were purchased from Sigma-Aldrich. Ammonium fluoride (98%) and ammonium hydroxide (25% solution in water) were purchased from Chem Supply. Zinc acetate dihydrate (99.5%) was purchased from Analar. Methoxyethanol (99.5%) and Super Yellow emitting polymer (livilux PDY-132) were purchased from Merck. PEDOT:PSS (Clevios HIL4) was purchased from Heraeus.

Seed Deposition: Zinc acetate was dissolved in methoxyethanol (0.5 M) in the presence of ethanolamine in a 1:1 molar ratio with zinc. Seed layers were deposited by spin coating at 2000 rpm for 30 s and then the films were annealed at 180 °C in air for 15 min on a hot plate.

Chemical Bath Deposition: The zinc stock solution was prepared by dissolving zinc nitrate in water and ammonia solution. The volume ratio between water and the ammonia solution was 10:1 and the final zinc concentration was 60×10^{-3} M. The stock solution of the ligand was prepared by dissolving ammonium citrate in water to give a 30×10^{-3} M concentration. The stock solution for the additive was prepared by dissolving ammonium fluoride in water to give a 75×10^{-3} M concentration.

The deposition experiments were undertaken using the Chemspeed SWINGXL automated synthetic platform. A full description of the configuration and operation of the robotics is included in the Supporting Information. In brief, appropriate amounts of the stock solutions were mixed together in empty glass vials at room temperature to achieve the desired amount of zinc, ligand and additive, and eventually diluted with deionized water to reach the required concentration. The molar ratio between the ligand and zinc (r_C) was varied between 0 and 0.5. The molar ratio between the additive and zinc (r_F) was varied between 0 and 1. The zinc concentration in the final solution ([Zn]) was varied between 5×10^{-3} and 20×10^{-3} M and the total volume of the solution was set at 15 mL. As an example, for the synthesis of a ZnO film with $r_C = 0.075$ and $r_F = 1$ at $[Zn] = 20 \times 10^{-3}$ M, 5 mL of the zinc stock solution, 0.75 mL of the ligand stock solution and 4 mL of the additive stock solutions were mixed together and diluted with a further 5.25 mL of water. The final solution was then transferred into preheated vials containing the substrate with the seeded surface facing slightly downward (Figure S1, Supporting Information). The temperature was controlled by recirculating oil in between heated plates and was verified by a thermocouple placed in a vial within the heated racks. Reactions were carried out at temperatures between 60 and 90 °C. All reactions were performed for 1 h, unless specified otherwise. A detailed list of the reaction conditions is provided in Table S2 (Supporting Information).

Once the deposition is finished, the samples are removed from the chemical bath and washed with deionized water and dried with a nitrogen stream. To remove possible surface precipitates, the samples were sonicated in ethanol for 3 min.

Post-treatment: ZnO films were exposed to UV light using a Novascan PSD-UVT UV-ozone cleaner operated at room temperature. Flash lamp exposure was done using a Xenon Sinteron 2010 system operated at 3 kV with 2 ms light pulses. The resting time between each pulse is set to 3 s, and the samples remained around room temperature for the whole duration of the flash tests.

Device Fabrication: After chemically etching ZnO films grown on glass using a 0.2 M solution of hydrochloric acid in water to define a pattern, the films were thoroughly washed with water, acetone, and isopropyl alcohol, and then exposed to 100 flash lamp pulses. The ZnO/glass substrates were transferred into a nitrogen-filled glove box and then PEDOT:PSS (Clevios HIL4) and Super Yellow (PDY-132, dissolved in toluene at 5 g L^{-1}) were deposited by spin coating to achieve thicknesses of ≈130 and 80 nm, respectively. The samples were annealed at 140 °C for 3 min after each layer to remove the solvents, and then the Ca (6 nm)/Ag (100 nm) metal cathode was thermally evaporated through a shadow mask defining pixels with an active area of 10 mm^2.

Characterization: The surface and cross-sectional morphology of the films deposited on silicon was investigated using an FEI Helios Nanolab 600 Scanning Electron Microscope (SEM). The thicknesses of the samples were evaluated using a Veeco Dektak 6M profilometer and confirmed by SEM on selected samples. XRD patterns of the deposited films were collected using a Bruker D8 diffractometer equipped with a Cu-Kα radiation source and operated at 40 kV and 40 mA. Optical absorption spectra of films deposited on glass substrates were measured using a Perkin-Elmer Lambda 1050 spectrophotometer equipped with an integrating sphere. Sheet resistances of the ZnO films deposited on glass were measured by using a Jandel RM3000 four-point probe and averaged over at least 5 measurements per sample. XPS analysis was performed using an AXIS Ultra DLD spectrometer (Kratos Analytical Inc., Manchester, UK) with a monochromated Al Kα source at a power of 144 W (12 kV × 12 mA), a hemispherical analyzer operating in the fixed analyzer transmission mode and the standard aperture (analysis area: 0.3 mm × 0.7 mm). The total pressure in the main vacuum chamber during analysis was typically between 10^{-9} and 10^{-8} mbar. Survey spectra were acquired at a pass energy of 160 eV. To obtain more detailed information, high-resolution spectra were recorded from individual peaks at 20 eV pass energy. Each specimen was analyzed at an emission angle of 0° as measured from the surface normal. Assuming typical values for the electron attenuation length of relevant photoelectrons, the XPS analysis depth (from which 95% of the detected signal originates) ranges between 5 and 10 nm for a flat surface. XPS data processing was performed using CasaXPS processing software version 2.3.15 (Casa Software Ltd., Teignmouth, UK). All elements present were identified from survey spectra. The atomic concentrations of the detected elements were calculated using integral peak intensities and the sensitivity factors supplied by the manufacturer. The individual components of the O 1s peak arising from chemically different species were assumed to have a Gaussian/Lorentzian lineshape and were quantified using nonlinear least-squares regression. The accuracy associated with quantitative XPS

is ≈10%–15%. Precision (i.e., reproducibility) depends on the signal/noise ratio but is usually much better than 5%. The latter is relevant when comparing similar samples. The voltage–current–luminance (*V–I–L*) measurements and the Commission International d'Eclairage (CIE) chromaticity coordinates (*x*,*y*) of the light emitting devices were tested using a Keithley 2400 SourceMeter and TOPCON BM-7A luminance colorimeter (0.2° measurement angle). The forward emission spectrum was recorded normal to the substrate with an optical fiber coupled to a calibrated ASEQ Instruments LR1 compact spectrometer.

Supporting Information

Supporting Information is available from the Wiley Online Library or from the author.

Acknowledgements

This work was funded through the Manufacturing Flagship of CSIRO as part of an Office of the Chief Executive Postdoctoral Fellowship (E.D.G.). J.J.J. acknowledges the Australian Research Council for funding through the grant DP110105341. Part of this work was performed at the Melbourne Centre for Nanofabrication (MCN) in the Victorian Node of the Australian National Fabrication Facility (ANFF).
Note: Figure 2 and 5 were amended on December 16, 2015.

Received: August 14, 2015
Revised: September 23, 2015
Published online: November 5, 2015

[1] B. C. Bunker, P. C. Rieke, B. J. Tarasevich, A. A. Campbell, G. E. Fryxell, G. L. Graff, L. Song, J. Liu, J. W. Virden, G. L. McVay, *Science* **1994**, *264*, 48.
[2] I. A. Aksay, M. Trau, S. Manne, I. Honma, N. Yao, L. Zhou, P. Fenter, P. M. Eisenberger, S. M. Gruner, *Science* **1996**, *273*, 892.
[3] F. F. Lange, *Science* **1996**, *273*, 903.
[4] R. A. Caruso, M. Antonietti, *Chem. Mater.* **2001**, *13*, 3272.
[5] B. Sun, H. Sirringhaus, *Nano Lett.* **2005**, *5*, 2408.
[6] T. P. Bigioni, X.-M. Lin, T. T. Nguyen, E. I. Corwin, T. A. Witten, H. M. Jaeger, *Nat. Mater.* **2006**, *5*, 265.
[7] J. Li, C. Daniel, D. Wood, *J. Power Sources* **2011**, *196*, 2452.
[8] B. A. Ridley, B. Nivi, J. M. Jacobson, *Science* **1999**, *286*, 746.
[9] J. Burschka, N. Pellet, S.-J. Moon, R. Humphry-Baker, P. Gao, M. K. Nazeeruddin, M. Gratzel, *Nature* **2013**, *499*, 316.
[10] Y. Sun, J. A. Rogers, *Adv. Mater.* **2007**, *19*, 1897.
[11] A. C. Arias, J. D. MacKenzie, I. McCulloch, J. Rivnay, A. Salleo, *Chem. Rev.* **2010**, *110*, 3.
[12] M.-G. Kim, M. G. Kanatzidis, A. Facchetti, T. J. Marks, *Nat. Mater.* **2011**, *10*, 382.
[13] J. Meyer, S. Hamwi, M. Kröger, W. Kowalsky, T. Riedl, A. Kahn, *Adv. Mater.* **2012**, *24*, 5408.
[14] W. F. Maier, K. Stöwe, S. Sieg, *Angew. Chem. Int. Ed.* **2007**, *46*, 6016.
[15] E. M. Chan, C. Xu, A. W. Mao, G. Han, J. S. Owen, B. E. Cohen, D. J. Milliron, *Nano Lett.* **2010**, *10*, 1874.
[16] R. Potyrailo, K. Rajan, K. Stoewe, I. Takeuchi, B. Chisholm, H. Lam, *ACS Comb. Sci.* **2011**, *13*, 579.
[17] N. M. K. Tse, D. F. Kennedy, B. A. Moffat, N. Kirby, R. A. Caruso, C. J. Drummond, *ACS Comb. Sci.* **2012**, *14*, 443.
[18] X. Mulet, C. E. Conn, C. Fong, D. F. Kennedy, M. J. Moghaddam, C. J. Drummond, *Acc. Chem. Res.* **2013**, *46*, 1497.
[19] L. Vayssieres, K. Keis, S.-E. Lindquist, A. Hagfeldt, *J. Phys. Chem. B* **2001**, *105*, 3350.
[20] Z. R. Tian, J. A. Voigt, J. Liu, B. McKenzie, M. J. McDermott, M. A. Rodriguez, H. Konishi, H. Xu, *Nat. Mater.* **2003**, *2*, 821.
[21] K. Govender, D. S. Boyle, P. B. Kenway, P. O'Brien, *J. Mater. Chem.* **2004**, *14*, 2575.
[22] L. E. Greene, M. Law, D. H. Tan, M. Montano, J. Goldberger, G. Somorjai, P. Yang, *Nano Lett.* **2005**, *5*, 1231.
[23] X. Liu, M. Afzaal, K. Ramasamy, P. O'Brien, J. Akhtar, *J. Am. Chem. Soc.* **2009**, *131*, 15106.
[24] J. Joo, B. Y. Chow, M. Prakash, E. S. Boyden, J. M. Jacobson, *Nat. Mater.* **2011**, *10*, 596.
[25] E. Della Gaspera, J. van Embden, A. S. R. Chesman, N. W. Duffy, J. J. Jasieniak, *ACS Appl. Mater. Interfaces* **2014**, *6*, 22519.
[26] Y.-Z. Long, M. Yu, B. Sun, C.-Z. Gu, Z. Fan, *Chem. Soc. Rev.* **2012**, *41*, 4560.
[27] C. Wang, R. Cheng, L. Liao, X. Duan, *Nano Today* **2013**, *8*, 514.
[28] C.-H. Hsu, D.-H. Chen, *Nanotechnology* **2010**, *21*, 285603.
[29] R. Chandramohan, T. A. Vijayan, S. Arumugam, H. B. Ramalingam, V. Dhanasekaran, K. Sundaram, T. Mahalingam, *Mater. Sci. Eng. B* **2011**, *176*, 152.
[30] M. Miyake, H. Fukui, T. Hirato, *Phys. Status Solidi A* **2012**, *209*, 945.
[31] M. Kevin, G. W. Ho, *J. Mater. Chem. A* **2013**, *1*, 14239.
[32] H. Wang, S. Baek, J. Song, J. Lee, S. Lim, *Nanotechnology* **2008**, *19*, 075607.
[33] J. T. Chen, J. Wang, R. F. Zhuo, D. Yan, J. J. Feng, F. Zhang, P. X. Yan, *Appl. Surf. Sci.* **2009**, *255*, 3959.
[34] M. Mazilu, N. Tigau, V. Musat. *Opt. Mater.* **2012**, *34*, 1833.
[35] H. Hagendorfer, K. Lienau, S. Nishiwaki, C. M. Fella, L. Kranz, A. R. Uhl, D. Jaeger, L. Luo, C. Gretener, S. Buecheler, Y. E. Romanyuk, A. N. Tiwari, *Adv. Mater.* **2014**, *26*, 632.
[36] P. Fuchs, H. Hagendorfer, Y. E. Romanyuk, A. N. Tiwari, *Phys. Status Solidi A* **2015**, *212*, 51.
[37] C. Wöll, *Prog. Surf. Sci.* **2007**, *82*, 55.
[38] D. A. Melnick, *J. Chem. Phys.* **1957**, *26*, 1136.
[39] A. J. Morfa, B. I. MacDonald, J. Subbiah, J. J. Jasieniak, *Sol. Energy Mater. Sol. Cells* **2014**, *124*, 211.
[40] E. Della Gaspera, M. Bersani, M. Cittadini, M. Guglielmi, D. Pagani, R. Noriega, S. Mehra, A. Salleo, A. Martucci, *J. Am. Chem. Soc.* **2013**, *135*, 3439.
[41] E. Della Gaspera, A. S. R. Chesman, J. van Embden, J. J. Jasieniak, *ACS Nano* **2014**, *8*, 9154.
[42] T. J. Coutts, D. L. Young, X. Li, *MRS Bull.* **2000**, *25*, 58.
[43] G. Haacke, *J. Appl. Phys.* **1976**, *47*, 4086.
[44] A. Marrani, F. Caprioli, A. Boccia, R. Zanoni, F. Decker, *J. Solid State Electrochem.* **2014**, *18*, 505.
[45] R. G. Gordon, *MRS Bull.* **2000**, *25*, 52.
[46] J. Rousset, E. Saucedo, D. Lincot, *Chem. Mater.* **2009**, *21*, 534.
[47] F. Wang, J.-H. Seo, Z. Li, A. V. Kvit, Z. Ma, X. Wang, *ACS Appl. Mater. Interfaces* **2014**, *6*, 1288.
[48] D. S. Hecht, L. Hu, G. Irvin, *Adv. Mater.* **2011**, *23*, 1482.
[49] L. Luo, D. Bozyigit, V. Wood, M. Niederberger, *Chem. Mater.* **2013**, *25*, 4901.